Fast algorithm for chirp transforms with zooming-in ability and its applications

Xuegong Deng, Bipin Bihari, Jianhua Gan, Feng Zhao, and Ray T. Chen

Microelectronics Research Center, Department of Electrical and Computer Engineering, The University of Texas, Austin, Texas 78758

Received July 16, 1999; revised manuscript received December 7, 1999; accepted December 22, 1999

A general fast numerical algorithm for chirp transforms is developed by using two fast Fourier transforms and employing an analytical kernel. This new algorithm unifies the calculations of arbitrary real-order fractional Fourier transforms and Fresnel diffraction. Its computational complexity is better than a fast convolution method using Fourier transforms. Furthermore, one can freely choose the sampling resolutions in both x and u space and zoom in on any portion of the data of interest. Computational results are compared with analytical ones. The errors are essentially limited by the accuracy of the fast Fourier transforms and are higher than the order 10^{-12} for most cases. As an example of its application to scalar diffraction, this algorithm can be used to calculate near-field patterns directly behind the aperture, $0 \leqslant z < d^2/\lambda$. It compensates another algorithm for Fresnel diffraction that is limited to $z > d^2/\lambda N$ [J. Opt. Soc. Am. A **15**, 2111 (1998)]. Experimental results from waveguide-output microcoupler diffraction are in good agreement with the calculations.
 [S0740-3232(00)01704-X]
OCIS codes: 350.6980, 070.2590, 050.1590, 050.1940

1. INTRODUCTION

Responses of many physical systems can be described with chirp transforms (ChT's). For example, chirps on laser pulses,[1] scalar diffraction through a first-order optical system,[2–6] holographic lenses,[7] and Fresnel transforms[8] (FnT's) are the most frequently reported techniques used in scalar diffraction calculations. Recent developments in optical interconnects spurred by high-speed and huge-capacity optical communications include problems similar to those just mentioned.[9–12] One example of such a system is illustrated in Fig. 1, where the optical signal is transmitted from board to board and is detected by detectors located several tens of wavelengths away. The near-field diffraction pattern at the detector ends directly affects the performance of the interconnection. It is preferable to obtain complete information on the evolution of the optical signals along the interconnecting path. In addition, it is easy to show that fractional-order Fourier transforms[13] (FrFT's) can also be treated as chirp transforms. Therefore, an accurate, simple, and efficient numerical method will be beneficial in the use of these extensively employed formulas.

Some studies have been done on the numerical evaluation of Fresnel diffraction; two examples are the use of fast Fourier transforms (FFT's) and convolution techniques[14] and a discrete-Fourier-transform- (DFT-) like matrix method.[15,16] A number of algorithms are also specifically devised for FrFT's [17–21] whose properties have been intensively investigated both mathematically[3–5,22] and physically[23–25] in terms of their applications to optical beam propagation,[6] imaging,[24–26] diffraction,[27] and signal and image processing.[28–36] The relations among FnT's, DFT's, and FrFT's are also well established.[32,37,38] Our aim in this paper is to develop an efficient algorithm that unifies the evaluations of these formulas.

In this paper we describe a fast numerical algorithm that is based on the chirp-z transform[39,40] to calculate chirp transforms. It employs two FFT's with an analytical kernel, and its computational complexity is better than a fast convolution. In addition, one can freely choose the sampling resolutions in both x space (signal domain) and u space (transformed, or response domain) and zoom in on any portion of the data of interest. Zooming in may be very useful in studying fine structures of some chirp systems, for example, near-field diffraction.[41] The sampling condition will also be addressed under the restriction of the Nyquist theorem.

In Section 2, first we compare several physical systems that can be classified as chirp transforms and establish a general mathematical description. Then in Subsection 3.A we present a discrete form of the transform. The sampling condition and discussions on peeping any portion of the data in u space are mentioned at the end of the Subsection 3.A. Following the discretization of the integral form of the transform, we use similar techniques in the chirp-z transform and develop the concrete fast algorithm in Subsections 3.B and 3.C. In Section 4 we give some numerical examples to demonstrate the effectiveness of this algorithm. Some closed-form transforms such as a Gaussian function and rect(x/a) are tested in Subsection 4.A. In Subsection 4.B the algorithm is applied to zooming in on the Fresnel diffraction of a rectangular window around the focal plane. Experimental results are provided for comparison. Near-field diffraction patterns from a 1-to-48-waveguide fan-out interconnection layer were measured, and they corresponded well to

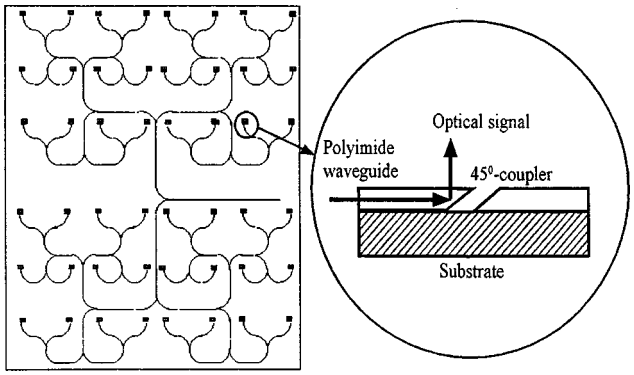

Fig. 1. Schematic top view of the H-tree waveguide used in optical interconnections. The side view of one of its 48 microcouplers is illustrated at the right. Near-field diffraction patterns of the outcoupling are critical to the coupling of the optical signal to detectors in successive layers and hence to the performance of the optical interconnections.

the results simulated with this algorithm in Subsection 4.C. In Subsection 4.D the versatility of this algorithm is demonstrated in calculating arbitrary real-order FrFT's.

2. COMPARISON OF SEVERAL GENERAL CHIRP TRANSFORM SYSTEMS

A chirp transform of an arbitrary signal $f(\mathbf{x})$ in an N-dimensional system is expressed by

$$g_{\mathrm{ch}}^{\mathbf{p}}(\mathbf{u}) \equiv \mathcal{C}^{\mathbf{p}}\{f(\mathbf{x})\} = \int_{-\infty}^{+\infty} f(\mathbf{x}) B_{\mathrm{ch}}^{\mathbf{p}}(\mathbf{u},\mathbf{x}) \mathrm{d}\mathbf{x}, \tag{1}$$

and the integration kernel is

$$B_{\mathrm{ch}}^{\mathbf{p}}(\mathbf{u},\ \mathbf{x}) \equiv \mathbf{A}(\mathbf{p}) \exp\left[-2\pi i \sum_{l=1}^{N} (\alpha_l x_l^2 + \beta_l x_l u_l + \gamma_l u_l^2) \right], \quad \mathbf{u},\ \mathbf{x} \in \mathcal{R}^{\mathbf{N}}, \tag{2}$$

where $A(\mathbf{p})$ is the amplitude of the kernel and generally a complex value, $i \equiv \sqrt{-1}$, and $\mathbf{p} \equiv (\alpha,\ \beta,\ \gamma)$ are the parameters of the transform, each of them being an N-dimensional vector. This transform maps the signal in $\mathbf{x}$ space (signal domain) to $\mathbf{u}$ space (chirp space, or response domain). All variables are dimensionless. To simplify the discussion, we will use the one-dimensional form of the above equations from now on. However, all the conclusions and results are applicable to the higher-dimensional cases as well.

In comparison, the Fresnel formula of scalar diffraction through a general Gaussian (first-order) optical system can be expressed with the Collins formula,[2,6,42] in which the transforming kernel is a special case of chirp transforms [Eq. (1)], namely,

$$B_{\mathrm{FnT}}^{M}(u,x) \equiv \frac{-i}{B\lambda} \exp\left[\frac{ik}{2B} (Ax^2 - 2xu + Du^2) \right], \tag{3}$$

which is associated with a ray-transfer matrix,[2,42,43]

$$M \equiv \begin{bmatrix} A & B \\ C & D \end{bmatrix}, \qquad \det M = \pm 1. \tag{4}$$

In Eq. (3), $\lambda \equiv (2\pi)/k$ is the wavelength. This formula connects the paraxial parameters and the Fresnel diffraction of the system. It can be rewritten as a special case of chirp transforms when the corresponding parameters are used:

$$\mathbf{p} \equiv (\alpha,\ \beta,\ \gamma) = \frac{-k}{4\pi B}(A, -2, D),$$

$$A(\mathbf{p}) = \frac{-i}{B\lambda}. \tag{5}$$

Similarly, the kernel of a real-value κth-order FrFT, $B_{\mathrm{FrFT}}^{\kappa}$, is another special case of the chirp transform and can be written as[44]

$$B_{\mathrm{FrFT}}^{\kappa}(u,x) = \frac{\exp[-i(\phi_s - \phi)/2]}{(2\pi|\sin(\phi)|)^{1/2}} \times \exp\left\{ i \left[\frac{(u^2 + x^2)}{2} \cot\phi - ux \csc\phi \right] \right\}, \quad \kappa \neq 2n, \tag{6}$$

in which $\phi \equiv (\pi/2)\kappa$, $\phi_s = [(\pi/2)\mathrm{sign}(\sin\phi)]$ and n is an integer.[45] Apparently, the corresponding ChT's parameters are

$$\mathbf{p} \equiv (\alpha,\ \beta,\ \gamma) = \frac{-1}{4\pi}[\cot(\phi), -2\csc(\phi), \cot(\phi)],$$

$$A(\mathbf{p}) = \frac{\exp[-i(\phi_s - \phi)/2]}{(2\pi|\sin(\phi)|)^{1/2}}. \tag{7}$$

Therefore a general algorithm for chirp transform applies to computations of all these cases of Fresnel diffraction, the Collins formula, and FrFT's. To preset a suitable form for numerical calculation of any ChT, in Subsection 3.A we will derive a discrete form of Eq. (1), and in Subsection 3.B we will concentrate on developing the fast algorithm.

3. DEVELOPMENT OF A FAST NUMERICAL ALGORITHM FOR THE GENERAL CHIRP TRANSFORM

A. Discrete Form of the Chirp Transform

For numerical calculation of the ChT of an arbitrary function $f(x)$ except those having analytical forms, first Eq. (1) will be digitized. For simplicity, we will use the simplest equidistant sampling. The sample steps are denoted δx for the signal space and δu for the chirp space. The sample numbers N_x and N_u for x space and u space must be limited; they are not necessarily equal. Therefore the discretization of Eq. (1) may be given as

$$x \to n'\delta x \equiv \left(n - \frac{N_x}{2} \right) \delta x, \qquad n = 0, 1, 2, \ldots N_x - 1,$$

$$u \to k'\delta u \equiv \left(k - \frac{N_u}{2} \right) \delta u, \qquad k = 0, 1, 2, \ldots N_u - 1,$$

and

$$g_k^p = g_{\mathrm{ch}}^p(k\,\delta u) \approx \sum_{n=0}^{N_x-1} f_n B_D^p(k,n)\,\delta x,$$

$$B_D^p(k,n) \equiv A(p)\exp\{-2\pi i[\alpha(n'\,\delta x)^2 + \beta n' k'\,\delta x\,\delta u + \gamma(k'\,\delta u)^2]\}, \tag{8}$$

where $f_n = f(n'\,\delta x)$ and $B_D^p(k,n) = B_{\mathrm{ch}}^p(k'\,\delta u, n'\,\delta x)$. It can be seen that the parameterized ChT of $f(x)$ is equivalent to the Fourier transform of the modified function $f_m(x) \equiv f(x)\exp(-2\pi i\alpha x^2)$, with a simultaneous variable scaling in u space except for the difference of a complex phasor. This could be inferred from Eq. (2) and written as

$$g_{\mathrm{ch}}^p(u) \propto g(v) \equiv \mathcal{F}\{f_m(x)\} = \mathcal{F}\{f(x)\exp(-2\pi i\alpha x^2)\}, \tag{9}$$

where $v = \beta u$ and $\mathcal{F}$ denotes a Fourier transform.[46] This is a well-known technique and was used in deriving several properties of FrFT (for example, see Refs. 13, 37, and 38). Therefore, according to the Nyquist sampling theorem, if $f_m(x)$ is band limited (i.e., there exists a minimum value v_m, $g(v) = 0, |v| \geqslant v_m > 0$), the sampling step in x space must satisfy

$$\delta x \leqslant \frac{1}{2v_m} \equiv \frac{1}{2\beta u_m}. \tag{10}$$

This is one implicit form of the Nyquist sampling theorem in ChT spaces.[34,47] Another explicit form of the sampling condition will be derived in Subsection 3.B. Under this restriction, one may correctly calculate the numerical transform of a given function.

If one is interested in the data peeping in u space and wants to scrutinize any region of $g_{\mathrm{ch}}^p(u)$, it may be instructive to look at the shifting rule of Fourier transforms. For any nontrivial ChT, $\beta \neq 0$, and any interested data window center c in u space,

$$g_{\mathrm{ch}}^p(u-c) \propto g(v-\beta c) = \mathcal{F}\{f_m(x)\exp[2\pi i\beta c x]\}. \tag{11}$$

The implementation for the data peeping is straightforward and needs no further discussion. In Subsection 3.B we will present the concrete fast procedure for numerical evaluation of the ChT.

B. Fast Numerical Algorithm for the Chirp Transform

The techniques used in the chirp-z transform[39,40] are also useful for efficient calculation of the ChT of a given function $f(x)$. Substituting the following expression into Eq. (8),

$$n'k' = -\tfrac{1}{2}[(n'-k')^2 - n'^2 - k'^2], \tag{12}$$

we get

$$B_D^p(k,n) = A(p)P_n^p Q_k^p B_{\mathrm{convol}}^p(n'-k'),$$

where the phasorlike P_n^p and Q_k^p, as well as the modified kernel $B_{\mathrm{convol}}^p(n'-k')$ are

$$P_n^p = \exp\left[-2\pi i\left(\alpha\,\delta x^2 - \frac{\beta}{2}\,\delta x\,\delta u\right)(n')^2\right],$$

$$Q_k^p = \exp\left[-2\pi i\left(\gamma\,\delta u^2 - \frac{\beta}{2}\,\delta x\,\delta u\right)(k')^2\right], \tag{13}$$

$$B_{\mathrm{convol}}^p(n'-k') = \exp[\pi i\beta(n'-k')^2\,\delta x\,\delta u].$$

Substituting Eq. (13) into Eq. (8), one can obtain

$$g_k^p = A(p)\,\delta x\left[\sum_{n=0}^{N_x-1} f_n^{(m)} B_{\mathrm{convol}}^p(n'-k')\right] Q_k^p, \tag{14}$$

where $f_n^{(m)} = f_n P_n^p$ is the modified discrete signal. Therefore the discrete ChT of f_n can be efficiently calculated through a fast convolution algorithm by use of FFT's such as the techniques in Refs. 17 and 39 which are straightforward and simple to implement. We can write the procedure symbolically as

$$g_k^p = A(p)\{\mathcal{F}^{-1}\{\mathcal{F}\{f_n^{(m)}\}\mathcal{F}\{\delta x B_{\mathrm{convol}}^p(n')\}\}Q_k^p. \tag{15}$$

$\mathcal{F}$ denotes a FFT and $\mathcal{F}^{-1}$ an inverse FFT. However, this is not the most efficient method. The transforming kernel is actually a generalized Gaussian function whose Fourier transform has a closed form,[48] i.e.,

$$\mathcal{F}\{\exp(-ax^2)\} = \sqrt{\frac{\pi}{a}}\exp\left[-\frac{(\pi u)^2}{a}\right], \qquad \mathcal{R}\{a\} \geqslant 0, \tag{16}$$

which, when applied to Eq. (15), becomes

$$\hat{B}_{\mathrm{convol}}^p(k) = \mathcal{F}\{\delta x B_{\mathrm{convol}}^p(n')\} = \sqrt{\frac{i\,\delta x}{\beta\,\delta u}}\exp\left(-\pi i\frac{u^2}{\beta\,\delta x\,\delta u}\right), \qquad \mathcal{R}\left\{\frac{i}{\beta}\right\} \geqslant 0. \tag{17}$$

For the discrete transform, suppose that the sampling number in x space is $L_x \geqslant N_x$ and the Fourier transform of the kernel on the u grids is

$$\hat{B}_{\mathrm{convol}}^p(k) = \sqrt{\frac{i\,\delta x}{\beta\,\delta u}}\exp\left[-\pi i\frac{1}{\beta\,\delta x\,\delta u}\left(\frac{k'}{L_x}\right)^2\right],$$

$$k' \equiv k - \frac{L_x}{2}, \quad k = 0, 1, 2, \ldots, L_x - 1. \tag{18}$$

The discrete ChT of Eq. (15) can be rewritten as

$$g_k^p = A(p)\{\mathcal{F}^{-1}\{\mathcal{F}\{f_n^{(m)}\}\hat{B}_{\mathrm{convol}}^p(k)\}Q_k^p\}. \tag{19}$$

For implementation of this algorithm, the sampling of the $\hat{B}_{\mathrm{convol}}^p(k)$ in u space must be so dense that the kernel is well approximated. In practice, this condition may be satisfied by

$$\frac{1}{\beta\,\delta x\,\delta u}\left(\frac{1}{L_x}\right)^2 \ll 1. \tag{20}$$

It has been assumed that the FFT's of the functions involved do exist. However, these functions can be a distribution (for example, the Dirac delta function) if we take the Fourier transforms in a general sense. Therefore one need not resort to mathematically rigorous conditions of the fast algorithm in practice by abiding by the sampling condition mentioned above. An alternative is to explicitly impose the restrictions of Eq. (17) on the parameter β.

One can easily verify that all the Fourier transforms are valid if the chirp transform in Eq. (1) exists.

The complexity of numerically evaluating Eq. (19) is about the same as that of two FFT's and no more than six sequential complex multiplications (including the possible data-peeping operation), namely, $2L_x[\log(L_x) + O(1)]$ (L_x is the number of FFT samples). Compared with the previous chirp-z techniques,[39,40] such as those used in Ref. 17, whose time complexity is exactly as that of Eq. (15), namely, $3L_x[\log(L_x) + O(1)]$, the improvement in computation time is about one third. Besides, with an analytical form, the accuracy will be much better. Some examples will be presented in Section 4. By using this algorithm, one can freely set the sampling steps in both x and u space, which is very useful under some circumstances such as examining near-field diffraction patterns and interpolation of sparse data in u space.[15,39] One can also choose different numbers of samples in x and u space by means of the implementation techniques in Subsection 3.C.

C. Implementation of the Fast Algorithm

To implement the algorithm, the most convenient and efficient way is probably to use the standard FFT's. Different numbers of samples in x and u space will be used in the following procedure.

Suppose that the original number of samples in x space is N_x and the required sampling number in u space is N_u, which can be different from N_x. Thus the length of a noncircular convolution is $L_{\text{convol}} = N_x + N_u - 1$, which is the minimum length that should be used for a FFT in Eq. (19). The sequence of calculations is summarized below.

1. Find a positive number $L_x \geqslant L_{\text{convol}}$ that makes $(L_x - N_x)$ an even number. L_x usually can take the lowest value that satisfies this requirement.
2. Then compute f_n and zero-pad $f_n^{(m)}$:

$$\mathcal{Z}\{f_n^{(m)}\}(n) = \begin{cases} 0 & 0 \leqslant n < \dfrac{(L_x - N_x)}{2} \\ f^{(m)}_{n-(L_x-N_x)/2} & \dfrac{(L_x - N_x)}{2} \leqslant n < \dfrac{(L_x + N_x)}{2} \\ 0 & \dfrac{(L_x + N_x)}{2} \leqslant n \leqslant L_x - 1 \end{cases}. \tag{21}$$

3. Compute the analytical kernel $\hat{B}^p_{\text{convol}}(k)$ by means of Eq. (18) for $k' = k - L_x/2$, $k = 0, 1, 2, \ldots, L_x - 1$.
4. Perform the fast convolution operation in Eq. (19):

$$C(l) = \mathcal{F}^{-}\{\mathcal{Z}\{f_n^{(m)}\}\}\hat{B}^p_{\text{convol}}(k)\}, \qquad l = 0, 1, 2, \ldots, L_x - 1. \tag{22}$$

5. Discard the first and last $(L_x - N_u)/2$ data of $C(l)$, and for $0 \leqslant k \leqslant N_u - 1$ let

$$g_k^p = A(p)Q_k^p C\left(k + \frac{L_x - N_u}{2}\right), \tag{23}$$

in which $(L_x - N_u)$ should be an even number. This constraint is not necessary, though it could be met easily in practice.

Similar procedures with minor modifications can be developed for arbitrary N_u. To simplify our discussion below, the equivalent requirement that N_x and N_u be of the same parity will be used. The performance of the algorithm will be evaluated with some application examples in Section 4.

4. APPLICATION EXAMPLES

To demonstrate the performance of this fast algorithm, we examine several chirp systems. Different samplings and resolutions are used for these systems. In addition, to unify our discussions, we define a scaling factor,

$$\zeta_{\text{zoom}} = \frac{\delta u}{\delta x}, \qquad \zeta_{\text{zoom}} > 0, \tag{24}$$

which defines the finesse of the zooming in. Its reciprocal, $1/\zeta_{\text{zoom}}$, is the magnification of the data window. For applications of data peeping or interpolation, $0 < \zeta_{\text{zoom}} \leqslant 1$, whereas zoom-out effects occur when $\zeta_{\text{zoom}} > 1$ under proper sampling; this topic will be addressed below.

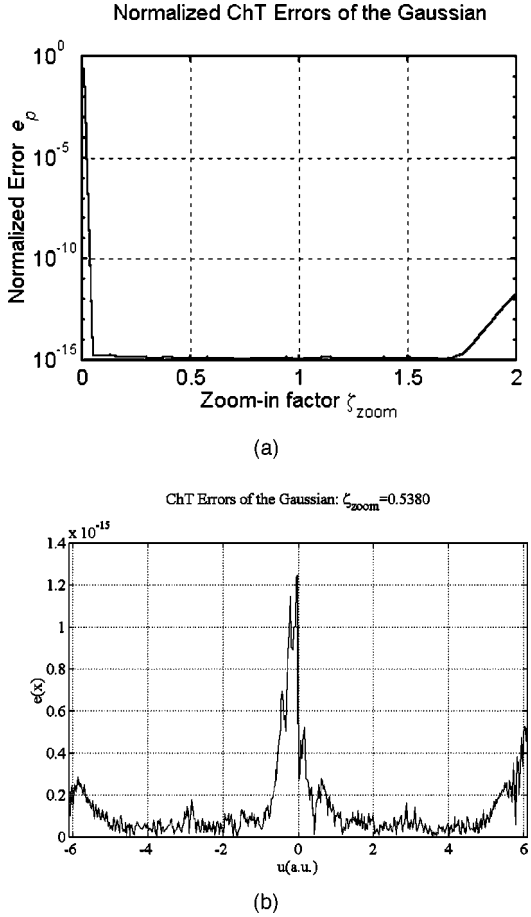

Fig. 2. (a) Errors $e_p = \max[e(x)]$ of the ChT's of a Gaussian function compared with the analytical transforms for different zoom factors ζ_{zoom}. (b) Typical error curve $e(x)$ ($\zeta_{\text{zoom}} = 0.5380$).

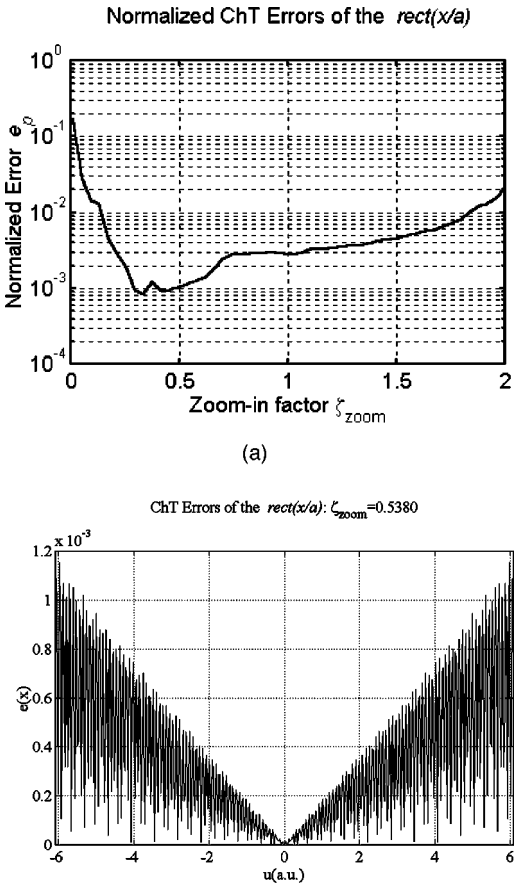

Fig. 3. (a) Errors max(e) of the ChT's of a rect(x/a) function compared with the analytical transforms for different zoom factors ζ_{zoom}. (b) Typical error curve $e(x)$ ($\zeta_{\text{zoom}} = 0.5380$).

A. Analytical Chirp Transforms

There are many functions whose ChT's are analytically available, such as a generalized Gaussian in Eq. (16). For simplicity, $\alpha = \gamma = 0$ and $R_x = \sqrt{N_x}$ were used. The ChT becomes a Fourier transform, and its space–bandwidth product[47,49] is N_x. We tested the fast algorithm with a Gaussian function for which $a^2 = \sqrt{\pi N_x}/(2R_x)$, where $x \in [-R_x/2, R_x/2]$, $N_x = N_u = 512$, and $L_x = N_x + N_u = 1024$. A normalized error measurement

$$e = \frac{|g_k^p - \mathcal{F}\{\exp(-ax^2)\}|}{\max(|g_k^p|)} \tag{25}$$

between the numerical result and the analytical one is used to check the accuracy. For different values of ζ_{zoom}, the ChT's and the corresponding $e_p \equiv \max(e)$ are plotted in Fig. 2(a), and a typical error curve for the ChT is plotted in Fig. 2(b). For $0.01 \leqslant \zeta_{\text{zoom}} < 2.0$, corresponding to a magnification of the data window of $0.5 \sim 100$, $e_p \approx 10^{-12}$.

A square function, rect(x/a), was used to test the algorithm. Its Fourier transform also has the closed form, $\mathcal{F}\{\text{rect}(x/a)\} = \sin(2\pi au)/\pi u$. For the same scaling factors, $a = R_x/4$, the ChT's as well as the accuracy measurement e_p are presented in Fig. 3(a). A typical error curve for the ChT is plotted in Fig. 3(b). The accuracy of the transform is much lower than that for a Gaussian, $e \approx 10^{-3}$. However, this does not decrease the validity and performance of the algorithm. Comparisons of Fig. 2(b), Fig. 3(b), and Fig. 4 indicate that most of the errors are accumulated in the FFT's used in the calculations. Therefore one can optimize the FFT parameters to achieve higher accuracy.[50]

B. Fresnel Diffraction of a Rectangular Window

The diffraction of a first-order optical system is perhaps one of the simplest chirp transforms but is not a trivial chirp one. In this section we calculate the well-known near-field diffraction of a rectangular window, rect($x/a, y/b$), behind an ideal focusing lens at different distances. The system is illustrated in Fig. 5(a), whose space–bandwidth product is discussed in Ref. 49. The elements of its ray-transfer matrix M are $A = 1 - l_2/f$, $B = l_1A + l_2$, $C = -1/f$, and $D = 1 - l_1/f$. In the simulations $N_x = 2N_u = 1024$, $\lambda = 0.85\,\mu$m, $a = 400\,\mu$m, $b = 200\,\mu$m, $l_1 = 1.0^{-8}\,\mu$m, $f = 5 \times 10^3\,\mu$m, and l_2 were varied from l_1 to $l_1 + f$ while ζ_{zoom} changed correspondingly.

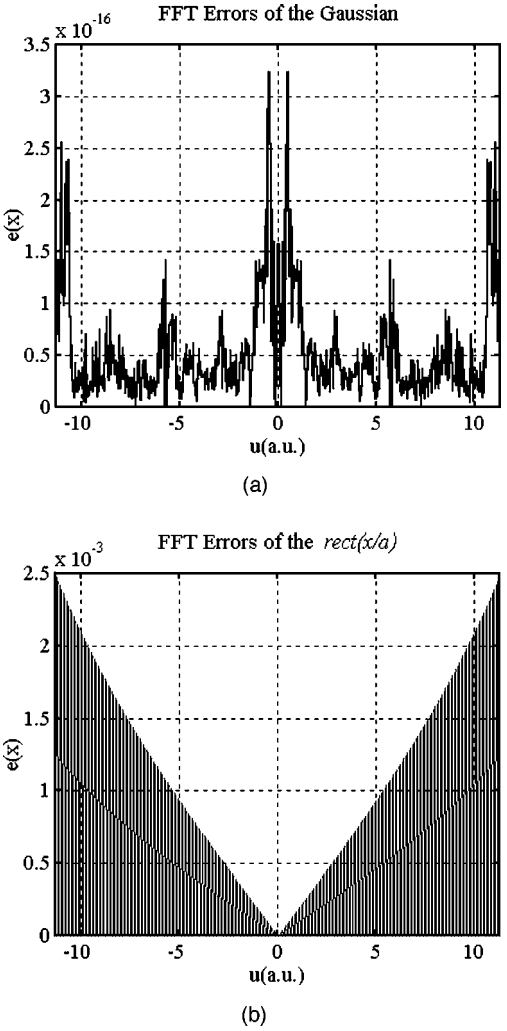

Fig. 4. Typical error curve of the FFT for (a) a Gaussian function, (b) rect(x/a).

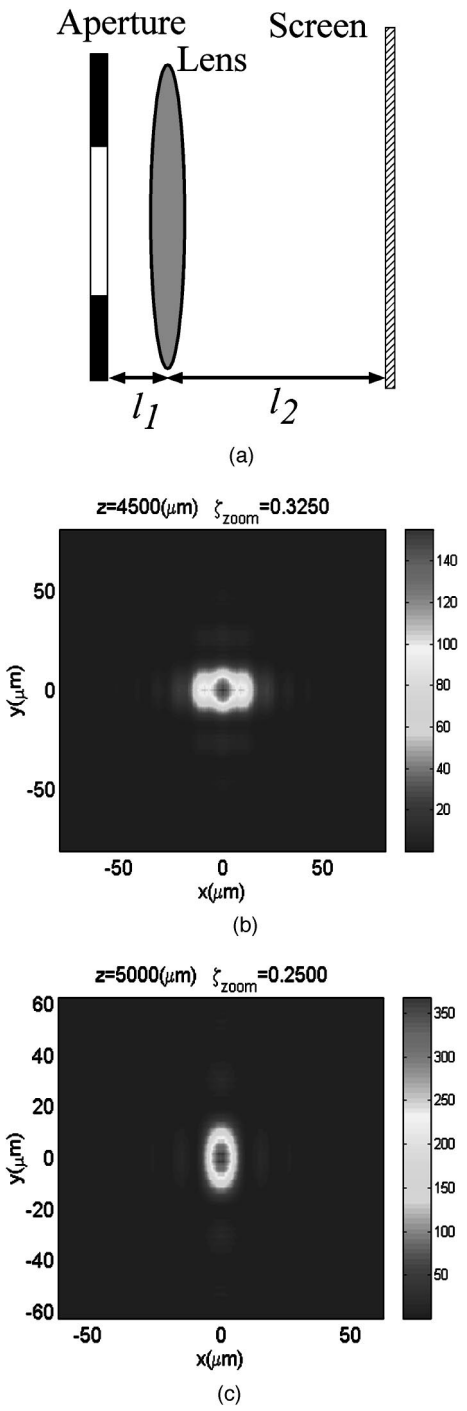

Fig. 5. Fresnel diffraction patterns of different zoom factors at different distances behind the aperture. (a) Layout of the optical system. Diffraction patterns for (b) $\zeta_{\text{zoom}} = 0.325$, $l_2 = 4500\ \mu$m and (c) $\zeta_{\text{zoom}} = 0.250$, $l_2 = 5000\ \mu$m.

A little trick can be employed for the x–y-separable cases like this one. In Cartesian coordinates, we can just use outer product of two one-dimensional ChT's in the x and y directions, i.e.,

$$u^M_{\text{diff}}(u_x, u_y) \equiv \mathcal{C}^M\{\text{rect}(x/a, y/b)\} = [\mathcal{C}^M\{\text{rect}(x/a)\}]^t \mathcal{C}^M\{\text{rect}(y/b)\}, \quad (26)$$

in which the one-dimensional transform is regarded as a row vector and the superscript t denotes its transpose. For nonseparable cases, one can directly use the one-dimensional ChT's and the techniques of multidimensional FFT's.[51] Two calculated diffraction patterns are depicted in Figs. 5(b) and 5(c). With the zoom-in factor changing with each distance, it is convenient to examine the fine structures near the focal regions as in Fig. 5(c) by using this fast algorithm.

C. Near-Field Outcoupling Patterns from a Waveguide

In another important application, we examine the near-field patterns of the outputs from the microcouplers in a 1-to-48 H-tree fan-out waveguide optoelectronics interconnection layer for massive clock signal distribution in a Cray T-90 supercomputer.[9] The optical layer of the system is illustrated in Fig. 1, where a side view of the structure of one of the 48 outcoupling points is schematically presented at the right. The polyimide waveguide is fabricated on a silicon substrate with 2-μm-thick silicon dioxide as bottom cladding. The waveguide is 65 μm wide[52] and 10 μm thick. The refractive index of the polyimide is $\sim$1.5364 at $\lambda = 1.310\ \mu$m for TE-polarized waves. The outcoupling window is a 45° slanted rectangular mirror.

The mode structure of the waveguide was calculated; its first ten eigenmodes in the 10 μm direction are plotted in Fig. 6. Matching the excitation boundary conditions for the waveguide indicate that multiple modes do exist in the waveguide. This finding validates the choice of a quasi-plane wave for the outcoupling wave at the outcoupling window in our calculations. For $\lambda = 0.850\ \mu$m, $N_x = 2N_u = 1024$, and $R_x = N_x \delta x = 10^3\ \mu$m, simulated results from the fast algorithm are depicted in Figs. 7(a), 7(b), 7(c), and 7(d) that correspond to the distances $z = 10^{-8}$, 100, 1000, and 5000 μm, respectively, surface normally above the waveguide. The zoom factor, ζ_{zoom}, were also changed along with the propagation distance. As a result of the divergence of the diffraction along the 10-μm side of the window, all zoom factors are greater than unity.

The diffracted patterns were measured at $z = 100$, 1000, and 5000 μm; they are presented in Figs. 7(e), 7(f), and 7(g), respectively. A detailed comparison of the experimental data with the calculations confirms our assumptions on the mode excitation of waveguide. The

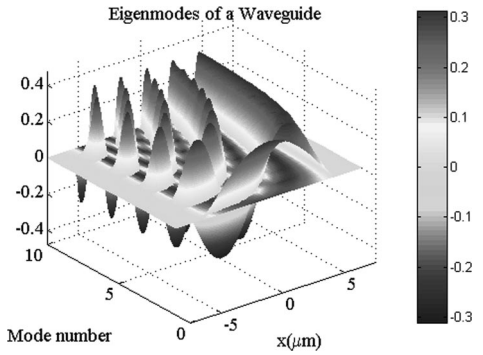

Fig. 6. First ten normalized eigenmodes in the 10 μm direction of the outcoupling points of the 1-to-48 fan-out H-tree polyimide waveguide. A slab waveguide model is used in the calculation because the width or the thickness of the waveguide is much larger than the wavelength.

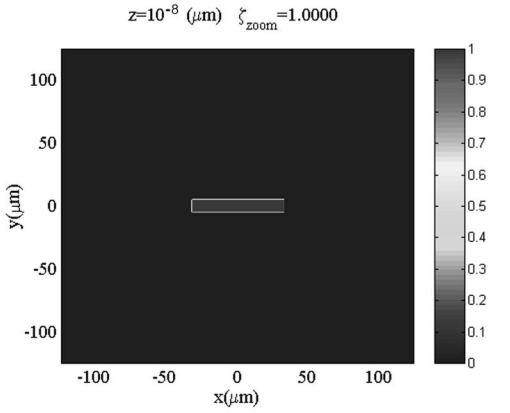

(a)

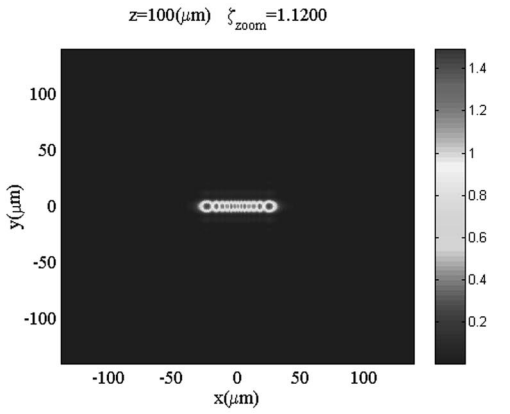

(b)

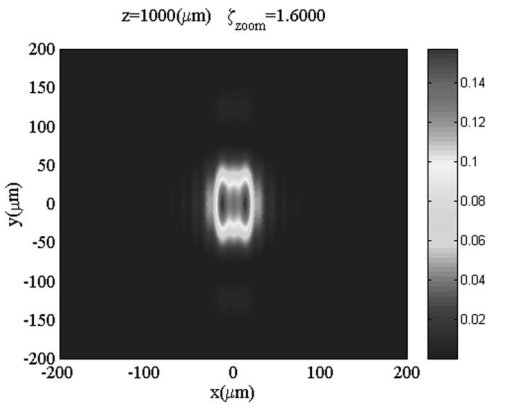

(c)

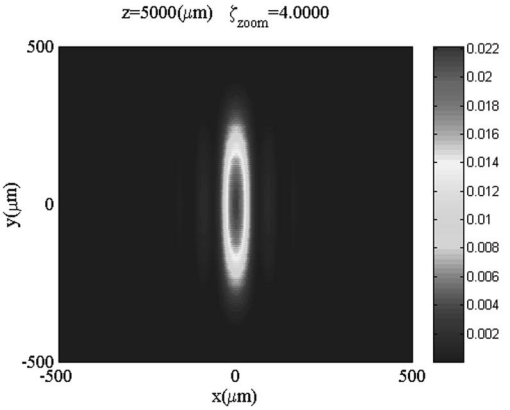

(d)

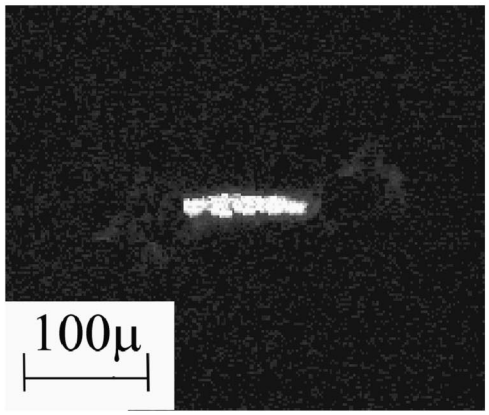

(e)

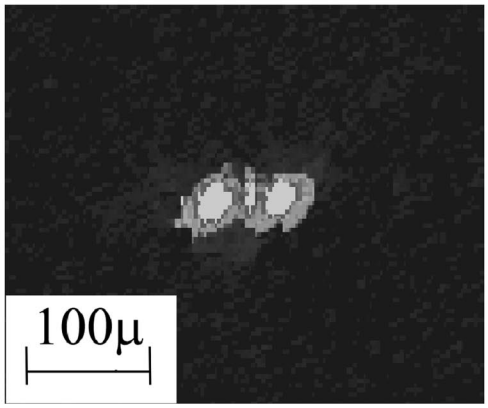

(f)

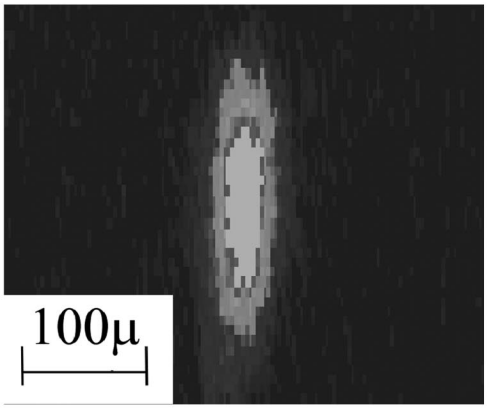

(g)

Fig. 7. Near-field outcoupling patterns from the waveguide as depicted in Fig. 1. Simulated results at (a) $z = 10^{-8}\ \mu$m, $\zeta_{\text{zoom}} = 1.000$; (b) $z = 100\ \mu$m, $\zeta_{\text{zoom}} = 1.120$; (c) $z = 1000\ \mu$m, $\zeta_{\text{zoom}} = 1.600$; (d) $z = 5000\ \mu$m, $\zeta_{\text{zoom}} = 4.000$. Experimental images corresponding to (e) $z = 100\ \mu$m, (f) $z = 1000\ \mu$m, and (g) $z = 5000\ \mu$m.

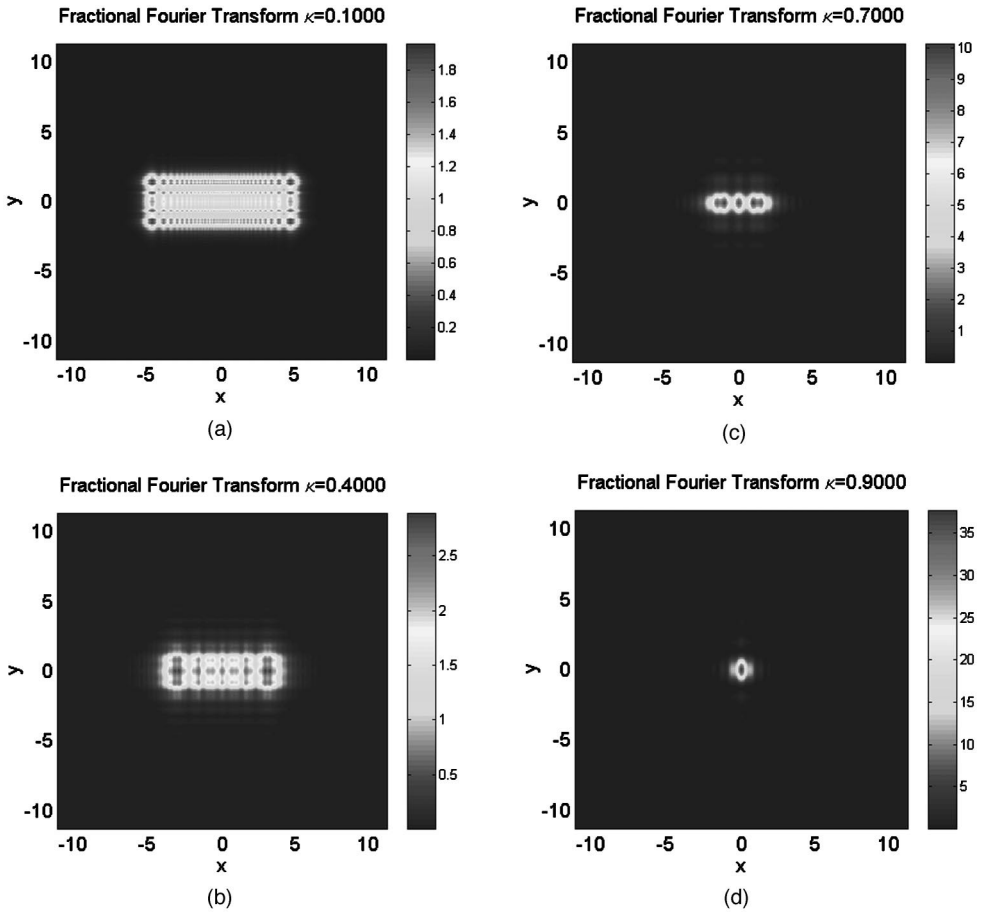

Fig. 8. FrFT's of a rectangular aperture, $\zeta_{\text{zoom}} = 1.0$. (a) $\kappa = 0.1$; (b) $\kappa = 0.4$; (c) $\kappa = 0.7$; (d) $\kappa = 0.9$.

spurious smaller dimensions in the experimental picture at $z = 5000\,\mu$m, i.e., Fig. 7(g), result from the fact that only the central lobe of the diffracted beam is visible, owing to background noise. A careful measurement of the lobe size as well as the sidelobe positions reveals the correct correspondence between the calculations and the experiments. For example, the vertical spot size is $\sim 268\,\mu$m as determined from experiments, and the calculated vertical spot size is $\sim 280\,\mu$m (the central gray region). Other characteristics such as nonzero regions from the central lobe to the first-order spots in the horizontal central region are also correctly located.

It is worth pointing out that the calculations for the above two applications are carried out for distances ranging from essentially zero behind the aperture to the focal plane or the far field; these calculations compensate another algorithm for Fresnel diffraction.[15] In Ref. 15 the applicable distance is limited to $z > d^2/\lambda N$, where $d = N_x \delta x$ is the aperture size and N is the sampling number. However, the sampling requirement of our algorithm, namely, Eq. (20), is equivalent to

$$\frac{1}{\beta \delta x\, \delta u L_x^2} = \frac{\lambda B}{(N_x \delta x)^2 \zeta_{\text{zoom}} (L_x/N_x)^2} \ll 1, \qquad (27)$$

in which we have plugged in Eq. (5). For a free-space system, $B = z$. The applicable distance range compensates the distance range in Ref. 15, $z \ll (N_x \delta x)^2/\lambda \zeta_{\text{zoom}} (L_x/N_x)^2 \sim R_x^2/\lambda$. The associated errors for scalar diffraction and its validity are analyzed in Refs. 8 and 53, and references therein.

D. Fractional Fourier Transform of Arbitrary Orders

The transverse distribution of the light propagating in one kind of graded-index fiber can be described with continuous order FrFT's.[30,54] As in Subsection 4.B, the incident wave is chosen as a plane wave on the rectangular aperture. For the fractional orders of $\kappa = 0.1$, 0.4, 0.7, 0.9, the x and u space are normalized so that the windows for calculation are $R_x = N_x \delta x = R_u = N_u \delta u = \sqrt{N_x}$. The size of the transparent aperture is $0.2R_x \times 0.5R_x$. The intensity of the FrFT's of the field is plotted in Fig. 8. Note that for $\kappa = 1.0$ the FrFT is just an ordinary Fourier transform. One may refer to Refs. 15 and 30 for comparisons. In this case the domain of interest for most cases is in the same range except for those with $\kappa = 2n + 1$. Therefore we have set the zoom-in factor $\zeta_{\text{zoom}} = 1.0$ regardless of the possible need to examine the details of the transformation.

On the free choice of the resolutions, there is an uncertainty principle in addition to the explicit restrictions such as Eq. (20). The least product of space–bandwidth for a FrFT system satisfies[32,38]

$$(\langle x^2 \rangle \langle u^2 \rangle)^{1/2} \geqslant \frac{1}{4\pi}. \qquad (28)$$

5. CONCLUSIONS

Employing some techniques formerly used in chirp-z transforms, we have derived a general fast algorithm for the numerical evaluation of chirp transforms. This algorithm employs two fast Fourier transforms (FFT's) and an analytical Gaussian kernel. The new algorithm is also suitable for the calculation of arbitrary real-order fractional Fourier transforms and scalar-field diffraction in first-order optical systems. Its computation complexity is $2L_x[\log_2 L_x + O(1)]$ and is better than a fast convolution using Fourier transforms. In addition, one can freely choose the sampling resolutions in both x and u space under the restriction of the Nyquist sampling theorem and zoom in on any portion of the data of interest.

Computational results are compared with analytical ones. The errors are limited by the accuracy of the FFT's. Extensions of the algorithm to higher dimensions is straightforward.

Several application examples are presented to demonstrate the versatility of the algorithm. Experimental results from an H-tree waveguide for optical interconnections confirmed the simulations. The new algorithm is capable of calculating near-field patterns directly behind the aperture, $0 \leqslant z < d^2/\lambda$. It compensates another algorithm for Fresnel diffraction that is limited to $z > d^2/\lambda N$. We believe that it is a handy tool for many general scalar diffraction problems.

ACKNOWLEDGMENTS

Xuegong Deng thanks Yongping Li (University of Science and Technology of China, Hefei, China), Yongkang Guo, Jingqin Su, and Yixiao Zhang (University of Sichuan, Sichuan, China) for their private communications regarding one of our former studies on FrFT's. Thanks also go to Yuri Rzhanov (Heriot-Watt University, Edinburgh, UK) for his careful review of the aforementioned literature and for discussions on several existing implementations of FrFT's. This work is partly supported by the Defense Advanced Research Projects Agency, Ballistic Missile Defense Organization, the U.S. Air Force Office of Scientific Research, Cray Research, 3M Foundation, the Texas Advanced Technology Program, and the Optoelectronics Industry Development Association Joint U.S.–Japan Optoelectronics Projects.

Corresponding author Ray T. Chen can be reached at the address on the title page or by phone, 512-471-7035; fax, 512-471-8575; or e-mail, raychen@uts.cc.utexas.edu.

REFERENCES AND NOTES

1. A. E. Siegman, *Lasers* (Mill Valley, Calif., 1986).
2. S. A. Collins, "Lens-system diffraction integral written in forms of matrix optics," J. Opt. Soc. Am. **60**, 1168–1177 (1970).
3. S. Abe and J. T. Sheridan, "Optical operations on wave functions as the Abelian subgroup of the special affine Fourier transformation," Opt. Lett. **19**, 1801–1803 (1994).
4. S. Abe and J. T. Sheridan, "Almost-Fourier and almost-Fresnel transformations," Opt. Commun. **113**, 385–388 (1995).
5. S. Abe, J. T. Sheridan, "Generalization of the fractional Fourier transformation to an arbitrary linear lossless transformation: an operator approach," J. Phys. A **27**, 4179–4187 (1994).
6. X. Deng, Y. Li, D. Fan, and Y. Qiu, "Propagation of paraxial flattened Gaussian beams in a general optical system," Opt. Commun. **140**, 226–230 (1997).
7. A. Katzir, A. C. Livanos, J. B. Shellan, and A. Yariv, "Chirped gratings in integrated optics," IEEE J. Quantum Electron. **QE-13**, 296–304 (1977).
8. G. W. Forbes, "Validity of the Fresnel approximation in the diffraction of collimated beams," J. Opt. Soc. Am. A **13**, 1816–1826 (1996).
9. B. Bihari, J. Gan, L. Wu, Y. Liu, S. Tang, and R. T. Chen, "Optical clock distribution in supercomputers using polyimide-based waveguides," in *Optoelectronic Interconnects VI*, J. P. Bristow and S. Tang, eds., Proc. SPIE **3632**, 123–133 (1999).
10. J. W. Goodman, F. I. Leonberger, S. Y. Kung, and R. A. Athale, "Optical interconnections for VLSI systems," Proc. IEEE **72**, 850–866 (1984).
11. P. Cinato and K. C. Young, Jr., "Optical interconnections within multichip modules," Opt. Eng. **32**, 852–860 (1993).
12. J. Jahns, "Planar integrated free-space optics," in *Micro-Optics: Elements, Systems and Applications*, H. P. Herzig, ed. (Taylor & Francis, London, UK, 1997), pp. 179–198; W. Singer and K. H. Brenner, "Stacked micro-optical systems," pp. 199–221.
13. V. Namias, "The fractional order Fourier transform and its application to quantum mechanics," J. Inst. Math. Appl. **25**, 241–265 (1980).
14. C. Kopp and P. Meyrueis, "Near-field Fresnel diffraction: improvement of a numerical propagator," Opt. Commun. **158**, 7–10 (1998).
15. S. B. Tucker, J. Ojeda-Castañeda, and W. T. Cathey, "Matrix description of near-field diffraction and the fractional Fourier transform," J. Opt. Soc. Am. A **16**, 316–322 (1999).
16. V. Arizón and J. Ojeda-Castañeda, "Fresnel diffraction of substructured gratings: matrix description," Opt. Lett. **20**, 118–120 (1995).
17. X. Deng, Y. Li, D. Fan, and Y. Qiu, "A fast algorithm for fractional Fourier transforms," Opt. Commun. **138**, 270–274 (1997).
18. F. J. Marinho and L. M. Bernardo, "Numerical calculation of fractional Fourier transforms with a single fast-Fourier-transform algorithm," J. Opt. Soc. Am. A **15**, 2111–2116 (1998).
19. H. Haman and J. L. de Bougrenet de la Tocnaye, "Efficient Fresnel-transform algorithm based on fractional Fresnel diffraction," J. Opt. Soc. Am. A **12**, 1920–1931 (1995).
20. B. W. Dickinson and K. Steigletz, "Eigenvectors and functions of the discrete Fourier transform," IEEE Trans. Acoust. Speech Signal Process. **ASSP-30**, 25–31 (1982).
21. S. C. Pei and M. H. Yeh, "Improved discrete fractional Fourier transform," Opt. Lett. **22**, 1047–1049 (1997).
22. G. S. Agarwal and R. Simon, "A simple relation of fractional Fourier transform and relation to harmonic oscillator Green's function," Opt. Commun. **110**, 23–26 (1994).
23. H. M. Ozaktas and D. Mendlovic, "Fourier transforms of fractional order and their optical implementation," Opt. Commun. **101**, 163–169 (1993).
24. A. W. Lohmann, "A fake zoom lens for fractional Fourier experiments," Opt. Commun. **115**, 437–443 (1995).
25. S. Liu, J. Xu, Y. Zhang, L. Chen, and C. Li, "General optical implementations of fractional Fourier transforms," Opt. Lett. **20**, 1053–1055 (1995).
26. L. M. Bernardo and O. D. D. Soares, "Fractional Fourier transform and imaging," J. Opt. Soc. Am. A **11**, 2622–2626 (1994).
27. P. Pellat-Finet, "Fresnel diffraction and the fractional Fourier transform," Opt. Lett. **19**, 1388–1390 (1994).
28. R. G. Dorsch, A. W. Lohmann, Y. Bitran, D. Mendlovic, and H. M. Ozaktas, "Chirp filtering in the fractional Fourier domain," Appl. Opt. **33**, 7599–7602 (1994).
29. D. Mendlovic and H. M. Ozaktas, "Fractional Fourier transforms and their optical implementations: I," J. Opt. Soc. Am. A **10**, 1875–1881 (1993).
30. H. M. Ozaktas and D. Mendlovic, "Fractional Fourier trans-

forms and their optical implementations. II," J. Opt. Soc. Am. A **10**, 2522–2531 (1993).
31. S. Granieri, O. Trabocchi, and E. E. Sicre, "Fractional Fourier transform applied to spatial filtering in the Fresnel domain," Opt. Commun. **119**, 275–278 (1995).
32. H. M. Ozaktas, B. Barshan, D. Mendlovic, and L. Onural, "Convolution, filtering, and multiplexing in fractional Fourier domains and their relation to chirp and wavelet transforms," J. Opt. Soc. Am. A **11**, 547–559 (1994).
33. D. Mendlovic, Y. Bitran, R. G. Dorsh, and A. W. Lohmann, "Optical fractional correlation: experimental results," J. Opt. Soc. Am. A **12**, 1665–1670 (1995).
34. D. Mendlovic, Z. Zalevsky, R. G. Dorsh, Y. Bitran, A. W. Lohmann, and H. M. Ozaktas, "New signal representation based on the fractional Fourier transform: definitions," J. Opt. Soc. Am. A **12**, 2424–2431 (1995).
35. H. M. Ozaktas, and D. Mendlovic, "Fractional Fourier optics," J. Opt. Soc. Am. A **12**, 743–751 (1995).
36. P. Pellat-Finet and G. Bonnet, "Fractional-order Fourier transform and Fourier optics," Opt. Commun. **111**, 141–154 (1994).
37. A. I. Zayed, "On the relationship between Fourier transform and fractional Fourier transform," IEEE Signal Process. Lett. **3**, 310–311 (1996).
38. A. W. Lohmann and B. H. Soffer, "Relationships between the Radon–Wigner and fractional Fourier transforms," J. Opt. Soc. Am. A **11**, 1789–1801 (1994).
39. S. Roose, B. Brichau and E. W. Stijns, "An efficient interpolation algorithm for Fourier and diffractive optics," Opt. Commun. **97**, 312–318 (1993).
40. L. R. Rabiner and B. Gold, *Theory and Applications of Digital Signal Processing* (Prentice-Hall, Englewood Cliffs, N.J., 1975).
41. M. Sypek, "Light propagation in the Fresnel region: new numerical approach," Opt. Commun. **116**, 43–48 (1995).
42. P. A. Béleuger, "Beam propagation and the *ABCD* ray matrix," Opt. Lett. **16**, 196–198 (1991).
43. A. Yariv, *Optical Electronics* (CBC College Publishing, New York, 1985), Chap. 2, pp. 17–52.
44. Y. B. Karasik, "Expression of the kernel of a fractional Fourier transform in elementary functions," Opt. Lett. **19**, 769–771 (1994).
45. For $\kappa = 2n$ the kernel becomes a Dirac delta function, $B_{\mathrm{FrFT}}^{(2n)}(u, x) = \delta[u - (-1)^n x]$, and the transform is straightforward and needs no further calculation.
46. To clarify the later results and be self-consistent, we will adopt the following definition of Fourier transform in the discrete form: Given $f(x)$, its Fourier transform is

$$g(u) \equiv \mathcal{F}\{f(x)\} = \int_{-\infty}^{\infty} f(x)\exp(-2\pi i x u)\mathrm{d}x,$$

which could be numerically approximated by

$$g(u) = \mathcal{F}\{f(x)\} \approx g_k = \sum_{l=0}^{N_x-1} f_n \exp[-2\pi i(n - N_x/2)(k - N_u/2)\delta x \delta u]\delta x.$$

We have assumed that the Fourier transform will map $f(x)$ from $x \in [-(N_x\delta x)/2, +(N_x\delta x)/2]$ to $g(u)$ in the domain $u \in [-(N_u\delta u)/2, +(N_u\delta u)/2]$. If g_k is given by a standard DFT or FFT, however, the mapped domain will be $u \in [-1/(2\delta x), +1/(2\delta x)]$ owing to the sampling condition $\delta x\,\delta u \equiv 1/N_x$.
47. A. W. Lohmann, R. G. Dorsch, D. Mendlovic, Z. Zalevshy, and C. Ferria, "Space–bandwidth product of optical signals and systems," J. Opt. Soc. Am. A **13**, 470–473 (1996).
48. I. S. Granshteyn and I. M. Ryzhik, *Table of Integrals, Series, and Products* (Academic, New York, 1985).
49. H. M. Ozaktas and H. Urey, "Space–bandwidth product of conventional Fourier transforming systems," Opt. Commun. **105**, 1–6 (1994).
50. L. Austander and F. A. Grünbaum, "The Fourier transform and the inverse Fourier transform," Inverse Probl. **5**, 149–164 (1989).
51. W. H. Press, S. A. Teukolsky, W. T. Vetterling, and B. P. Flannery, *Numerical Recipes in C: the Art of Scientific Computing* (Cambridge U. Press, Cambridge, UK, 1992).
52. The width of the mask used to fabricate the 10-μm-thick waveguide is 50 μm. Owing to the highly isotropic etching, the final width of the polyimide waveguide can be varied in the range of 60 $\sim$ 70 μm depending on the precise control of experiment environments. In our simulation, we used a typical value of 65 μm.
53. F. Depasse, M. A. Paesler, D. Courjon, and J. M. Vigoureux, "Huygens–Fresnel principle in the near field," Opt. Lett. **20**, 234–236 (1995).
54. A. Yariv, *Optical Electronics* (CBC College Publishing, New York, 1985).